CHEMISTRY
A EUROPEAN JOURNAL

DOI: 10.1002/chem.200902874

Noncovalent Assembly of Picket-Fence Porphyrins on Nitrogen-Doped Carbon Nanotubes for Highly Efficient Catalysis and Biosensing

Wenwen Tu,[a] Jianping Lei,*[a] Guoqiang Jian,[b] Zheng Hu,[b] and Huangxian Ju*[a]

Abstract: A water-insoluble picket-fence porphyrin was first assembled on nitrogen-doped multiwalled carbon nanotubes (CN_x MWNTs) through Fe–N coordination for highly efficient catalysis and biosensing. Scanning electron micrographs, Raman spectra, X-ray photoelectron spectra, UV/Vis absorption spectra, and electrochemical impedance spectra were employed to characterize this novel nanocomposite. By using electrochemical methods on the porphyrin at low potential in neutral aqueous solution, the presence of CN_x MWNTs led to the direct formation of a high-valent iron(IV)–porphyrin unit, which produced excellent catalytic activity toward the oxidation of sulfite ions. By using sulfite ions, a widely used versatile additive and preservative in the food and beverage industries, as a model, a highly sensitive amperometric biosensor was proposed. The biosensor showed a linear range of four orders of magnitude from 8.0×10^{-7} to $4.9\times10^{-3}\,mol\,L^{-1}$ and a detection limit of $3.5\times10^{-7}\,mol\,L^{-1}$ due to the highly efficient catalysis of the nanocomposite. The designed platform and method had good analytical performance and could be successfully applied in the determination of sulfite ions in beverages. The direct noncovalent assembly of porphyrin on CN_x MWNTs provided a facile way to design novel biofunctional materials for biosensing and photovoltaic devices.

Keywords: biosensors · catalysis · nanotubes · noncovalent assembly · porphyrinoids

Introduction

The functionalization of carbon nanotubes (CNTs) with porphyrins has attracted considerable attention for various applications due to their unique photophysical and photochemical properties.[1–11] Generally, this procedure can be performed by covalent or noncovalent routes. The noncovalent routes, including electrostatic interactions, π–π interactions, and axial coordination, are particularly promising for improving the dispersion or dissolution properties of CNTs without destructing the sp^2 nanotube structure. Both electrostatic and π–π noncovalent interactions of CNTs with porphyrins have been extensively applied in the preparation of photocatalytic and photovoltaic devices with excellent performance.[5–8] However, the functionalization of CNTs with porphyrins by axial coordination is very difficult due to the absence of sufficient binding sites on CNTs. To achieve the axial coordination for porphyrin functionalization of CNTs, pyridyl[9] and 4-aminopyridine[10] groups were covalently bound and the imidazole ligand assembled by π–π stacking interactions[11] to the surface of CNTs to form an electron donor for the self-assembly of acceptors, such as porphyrin molecules. This work used doping of heteroatoms, especially nitrogen atoms, in the carbon nanotube structure, which provided abundant binding sites for noncovalent functionalization, and prepared a functional nanocomposite of nitrogen-doped multiwalled carbon nanotubes (CN_x MWNTs) with a picket-fence porphyrin, bromo[iron(III) 5,10,15,20-tetrakis(α,α,α,α-2-pivalamidopheny)porphyrin] (FeTpivPP) through Fe–N coordination (Figure 1). This approach provided a facile avenue for the direct noncovalent assembly of the porphyrin and the design of novel biofunctional materials.

The CN_x MWNTs usually have a defective bamboolike structure with distinctive compartment layers due to the doping of nitrogen atoms bonded to the carbon atoms in two forms, namely, pyridinic and graphitic nitrogen atoms.

[a] W. Tu, Dr. J. Lei, Prof. H. Ju
MOE Key Laboratory of Analytical Chemistry for Life Science
School of Chemistry and Chemical Engineering
Nanjing University, Nanjing 210093 (China)
Fax: (+86) 25-8359-3593
E-mail: hxju@nju.edu.cn
jpl@nju.edu.cn

[b] G. Jian, Prof. Z. Hu
MOE Key Laboratory of Mesoscopic Chemistry
School of Chemistry and Chemical Engineering
Nanjing University, Nanjing 210093 (China)

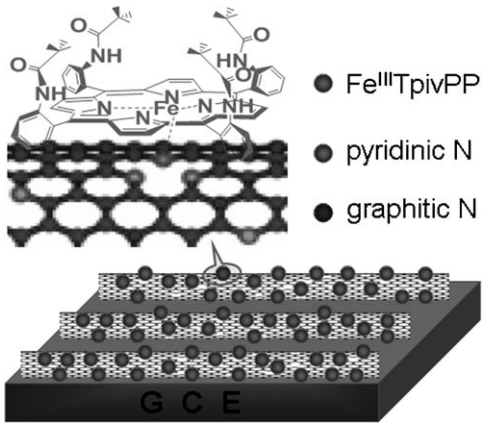

Figure 1. Proposed schematic diagram of the CN_x MWNTs/FeTpivPP-modified GCE.

In comparison with CNTs, CN_x MWNTs have a larger surface-active groups/volume ratio, better electrical and mechanical properties, and better biocompatibility.[12–15] The doped nitrogen atom can act as an electron donor and introduce some defective sites or active sites on the nanotube surface, which is expected to be an excellent candidate for fabricating nanocomposites.[16–19]

Porphyrins are an important class of conjugated organic molecule, which can be employed to mimic the active site of many important enzymes, such as hemoglobin, myoglobin, cytochrome c oxidase, nitric oxide reductase, vitamin B_{12}, and chlorophyll.[20–23] Metalloporphyrin has been well used as electron media and exhibited good electrocatalysis of many small molecules related to life process.[24–27] Especially, high-valent iron(IV)–porphyrin as a strong oxidant has been utilized to catalyze mono-oxygenation in many chemical reactions, including the catalytic oxidation of organic substrates and biomolecules.[28,29] In comparison with a plane porphyrin, a picket-fence porphyrin has a macrocyclic porphyrin ring with four columnlike phenyl substitutes, which simulates the active center of some proteins and enzymes, thus leading to improved catalysis toward biomolecules.[30–32] This investigation used FeTpivPP to functionalize CN_x MWNTs in the preparation of highly efficient catalysts. The presence of CN_x MWNTs led to a direct electron transfer from the porphyrin to the electrode to form a high-valent iron(IV)–porphyrin easily, thus producing excellent catalytic activity of the oxidation of sulfite ions with a low overpotential.

Sulfite ions are widely used as versatile additives and preservatives in the food and beverage industries to prevent oxidation and bacterial growth, control enzymatic reactions, and assist in preserving vitamin C during production and storage.[33] However, excess concentration of sulfite ions is harmful to the skin, respiratory tract, or stomach and intestines.[34–36] The United States Food and Drug Administration regulations have indicated that the sulfite ions contained in food and beverages (i.e., "contains sulfites") should not exceed 10 mg L^{-1}.[37,38] Therefore, effective monitoring of sulfite ions is urgently important.

On the basis of its catalytic activity, a sensitive amperometric biosensor with a low overpotential and a wide linear range for sulfite ions was designed. This biosensor could be successfully applied in the determination of sulfite ions in beverages. Therefore, the novel nanocomposite possesses potential applications as a highly efficient catalyst and in the fabrication of biosensors.

Results and Discussion

SEM and Raman spectroscopic characterization of CN_x MWNTs/FeTpivPP: The scanning electron micrograph of pristine CN_x MWNTs displayed a well-defined one-dimensional structure with the outer diameter of around 30 nm (Figure 2). This well-dispersed and interdigitated nanostructure provided a significant increase in the effective area for biomolecule loading. Furthermore, the Raman spectrum of pristine CN_x MWNTs showed a disorder-induced D band at $\lambda = 1357$ cm^{-1} and a tangential stretch G band at $\lambda = 1586$ cm^{-1} (Figure 3, curve a), with an intensity ratio I_D/I_G of 0.91. This value was much higher than 0.24 for undoped MWNTs,[39,40] thus indicating that the nitrogen doping was very effective in introducing defects into the structure of the CNTs. As a result, the obtained CN_x MWNTs had more defective sites for functionalization. In comparison with CN_x MWNTs, the D and G bands of CN_x MWNT/FeTpivPP were slightly shifted to $\lambda = 1353$ and 1583 cm^{-1} (Figure 3, curve b), respectively, which could be associated with FeTpivPP bound to the CN_x MWNTs. Moreover, the values of I_D/I_G for the CN_x MWNTs and CN_x MWNT/FeTpivPP did not show obvious differences, thus indicating that the func-

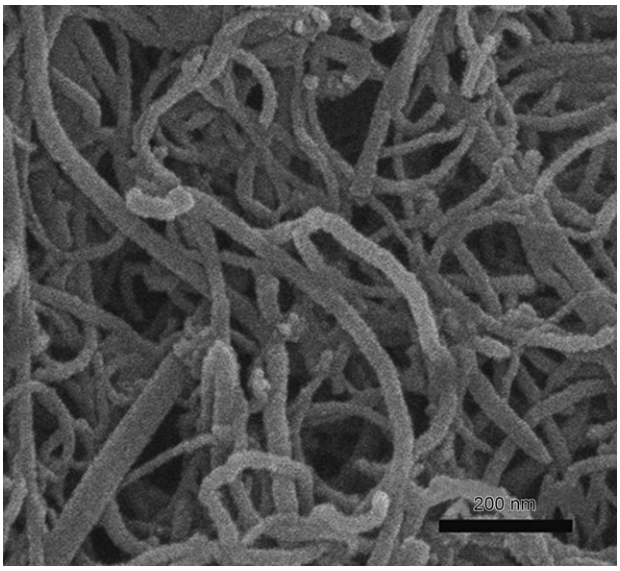

Figure 2. Scanning electron micrograph of pristine CN_x MWNTs.

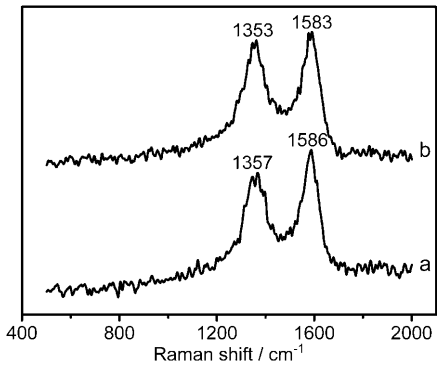

Figure 3. Raman spectra of a) CN_x MWNTs and b) CN_x MWNT/FeTpivPP.

tionalization of CN_x MWNTs with FeTpivPP did not destroy the structure of the CN_x MWNTs.

X-ray photoelectron spectrum (XPS) characterization of CN_x MWNT/FeTpivPP: The N 1s XPS of FeTpivPP consisted of two peaks assigned to the imido and pyrrolic nitrogen atoms at 399.0 and 400.2 eV, respectively (Figure 4A). The

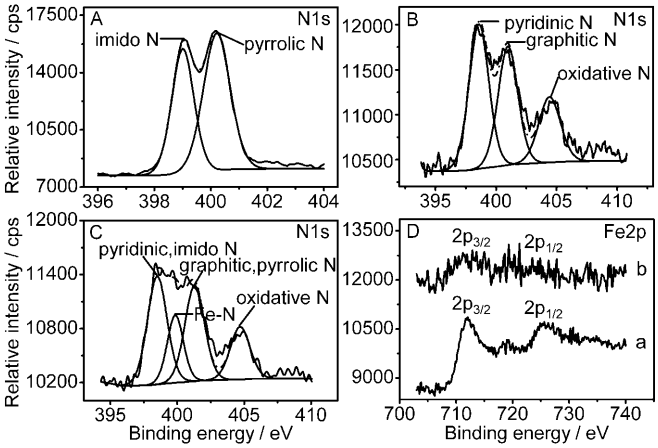

Figure 4. N 1s XPS of A) FeTpivPP, B) CN_x MWNTs, C) CN_x MWNT/FeTpivPP, and D) Fe 2p XPS of a) FeTpivPP and b) CN_x MWNT/FeTpivPP.

N 1s XPS of CN_x MWNTs exhibited three well-separated peaks attributed to the pyridinic, graphitic, and some oxidized nitrogen species at 398.6, 401.0, and 404.4 eV (Figure 4B).[41–43] In comparison with the XPS of CN_x MWNTs, CN_x MWNT/FeTpivPP showed a new peak at 399.8 eV (Figure 4C), which could been contributed to by the coordination between the Fe centers of FeTpivPP and the pyridinic nitrogen atoms of CN_x MWNTs. Moreover, after binding with FeTpivPP, the intensity ratio of the pyridinic and graphitic N 1s centers for CN_x MWNTs obviously decreased, thus indicating that part of the pyridinic nitrogen atoms of the CN_x MWNTs could be coordinated with the Fe center of FeTpivPP. This suggestion was also verified by comparing the Fe $2p_{2/3}$ peaks of Fe–N in FeTpivPP and CN_x MWNT/FeTpivPP. The former occurred at 711.7 eV (Figure 4D, curve a), and the latter shifted to a higher energy at 712.9 eV (Figure 4D, curve b). This shift should be attributed to the presence of electron-donating pyridinic nitrogen atoms of CN_x MWNTs that coordinate the central Fe atom of FeTpivPP. Thus, the nanocomposite of CN_x MWNT/FeTpivPP was formed through Fe–N coordination rather than only weak π–π noncovalent interactions.

UV/Vis absorption spectroscopic characterization of CN_x MWNT/FeTpivPP: The UV/Vis absorption spectra of FeTpivPP, MWNT/FeTpivPP, CN_x MWNT/FeTpivPP, the corresponding free-base porphyrin (H_2TpivPP), and CN_x MWNT/H_2TpivPP are shown in Figure 5A. The FeTpivPP exhibited

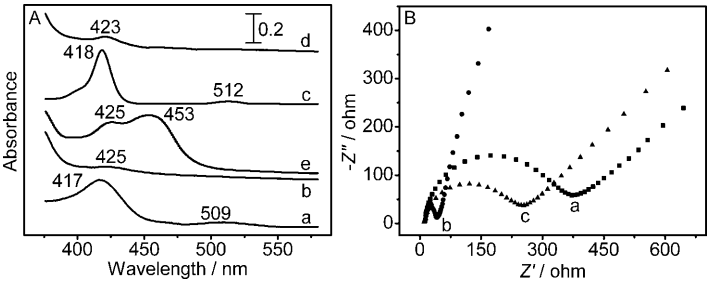

Figure 5. A) UV/Vis absorption spectra of a) FeTpivPP, b) MWNT/FeTpivPP, c) H_2TpivPP, d) CN_x MWNTs/H_2TpivPP, and e) CN_x MWNT/FeTpivPP. B) Electrochemical impedance spectra of a) bare, b) CN_x MWNTs, and c) CN_x MWNT/FeTpivPP-modified GCEs.

a typical Soret-band absorption at $\lambda = 417$ nm and a weak Q-band absorption at $\lambda = 509$ nm (Figure 5A, curve a), which was consistent with a previous report.[44] In the presence of MWNTs, the Soret band of MWNT/FeTpivPP showed a decrease in intensity with a red shift from $\lambda = 417$ to 425 nm, thus indicating the formation of a J-type aggregate nucleated on MWNTs through π–π noncovalent interactions (Figure 5A, curve b).[45] Similarly, the assembly of H_2TpivPP on CN_x MWNTs resulted in a slight shift of the Soret band of H_2TpivPP from $\lambda = 418$ to 423 nm (Figure 5A, curves c and d), whereas no split of the Soret band could be observed. However, in the presence of CN_x MWNTs, the Soret band of CN_x MWNT/FeTpivPP was split into two adsorption peaks at $\lambda = 425$ and 453 nm (Figure 5A, curve e), which could be attributed to the assembly of FeTpivPP on CN_x MWNTs by Fe–N coordination.[46]

Electrochemical impedance spectroscopic characterization of CN_x MWNT/FeTpivPP: After using the $[Fe(CN)_6]^{3-}$/$[Fe(CN)_6]^{4-}$ redox couple as the electrochemical probe, the Nyquist plots of different electrodes in the frequency range 0.01–100000 Hz were prepared (Figure 5B). On a bare glassy carbon electrode (GCE), the redox process of the probe showed an electron-transfer resistance of about 370 Ω (Figure 5B, curve a). After the CN_x MWNTs were coated onto the electrode, the resistance decreased dramatically to about 25 Ω (Figure 5B, curve b), thus suggesting that CN_x

MWNTs accelerated the electron transfer between the redox probe and electrode surface due to their excellent electronic conductivity. However, compared with CN_x MWNTs, the electron-transfer resistance of a CN_x MWNT/FeTpivPP-modified GCE was 230 Ω due to the presence of FeTpivPP, which blocked the electron transfer (Figure 5B, curve c). The increased electron-transfer resistance further demonstrated that FeTpivPP was assembled on CN_x MWNTs to form a noncomposite of CN_x MWNT/FeTpivPP.

Electrochemical behavior of the CN_x MWNT/FeTpivPP-modified GCE: The cyclic voltammogram of CN_x MWNT-modified GCE in N_2-saturated phosphate buffered saline (PBS) showed a couple of small redox peaks that resulted from oxycarbide species on the nanotube surface (Figure 6A, curve a). The CN_x MWNT/FeTpivPP-modified

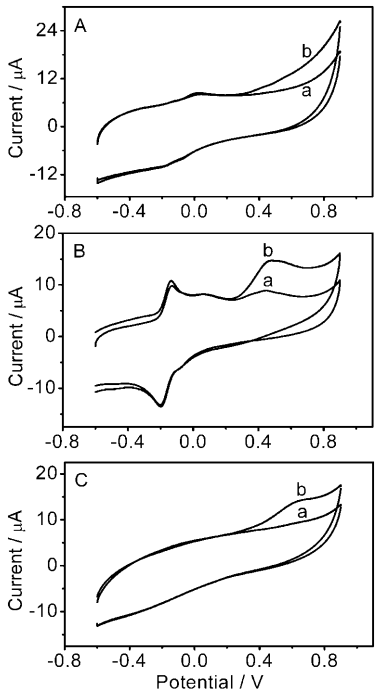

Figure 6. Cyclic voltammograms of GCEs modified with A) CN_x MWNTs, B) CN_x MWNT/FeTpivPP, and C) MWNT/FeTpivPP in a) N_2-saturated PBS (0.1 M, pH 7.0) and b) N_2-saturated PBS + sulfite (0.1 M, pH 7.0, 500 μmol L^{-1}) at 100 mV s^{-1}.

GCE showed another couple of well-defined redox peaks at −0.196 and −0.141 V and an anodic peak at +0.44 V (Figure 6B, curve a), whereas the cyclic voltammogram of the MWNT/FeTpivPP-modified GCE did not show any observable peak (Figure 6C, curve a). Thus, CN_x MWNTs could assemble much more FeTpivPP on their surface through Fe–N coordination, which showed stronger interactions than the π–π interaction between FeTpivPP and MWNTs. The redox peaks at lower potentials should be attributed to the redox couple of Fe^{III}/Fe^{II} with the separation of peak potentials ΔE_p of 0.055 V, which was smaller than that of ΔE_p = 0.115 V for a gold electrode modified with gold nanoparticles/MWNTs picket-fence porphyrin, [47] thus indicating that CN_x MWNTs promoted the electron transfer between FeTpivPP and the GCE. The reduction and oxidation peak currents of the CN_x MWNT/FeTpivPP-modified GCE increased linearly with a scan rate of 40–500 mV s^{-1}, whereas the difference in the redox peak potentials showed a slight increase that indicates a surface-controlled electrode process.

The irreversible oxidation peak observed at +0.44 V corresponded to the formation of an iron(IV) species.[48] The oxidation peak potential of Fe^{III}TpivPP was much more negative than +0.72 V for a GCE modified with iron(III) tetra(4-aminophenyl)porphyrin,[49] and +0.83 V for an indium/tin oxide electode modified with iron(III) *meso*-tetrakis(*N*-methylpyridinium-4-yl)porphyrin.[28] Moreover, the oxidation potential showed a strong dependence on the pH value of the solution. On increasing the solution from pH 5 to 9, the oxidation potential linearly shifted to more negative value with a slope of −55.2 mV pH^{-1}, thus indicating that one proton participated in the one-electron redox process [Eq. (1)]:

$$HO{-}Fe^{III}TpivPP - e^- \rightarrow O{=}Fe^{IV}TpivPP + H^+ \quad (1)$$

Electrocatalytic oxidation of sulfite ions: When sulfite ions (500 μmol L^{-1}) were added to PBS, an enhanced catalytic peak toward the oxidation of sulfite ions was observed at +0.47 V with the initial potential of +0.23 V at the CN_x MWNT/FeTpivPP-modified GCE (Figure 6B, curve b), whereas no obvious peak for the oxidation of sulfite ions was observed at the CN_x MWNT-modified GCE (Figure 6A, curve b). This result suggested that the CN_x MWNT/FeTpivPP nanocomposite greatly decreased the overpotential for the electrooxidation of sulfite ions due to the presence of $O{=}Fe^{IV}$TpivPP. As expected, the sulfite ions showed a weak electrooxidation peak at the MWNT/FeTpivPP-modified GCE (Figure 6C, curve b), thus indicating that little FeTpivPP had assembled on the MWNTs surface again due to the weaker π–π interactions than the Fe–N coordination on the CN_x MWNTs surface. Comparison of the responses of the sulfite ions on the CN_x MWNTs and CN_x MWNT/FeTpivPP-modified GCEs, the electrocatalytic oxidation of the sulfite ions was attributed to the iron(IV) center of FeTpivPP rather than the presence of the residual Fe catalyst in the CN_x MWNTs. This result suggests that the CN_x MWNT/FeTpivPP nanocomposite greatly decreased the overpotential for the electrooxidation of sulfite ions due to the presence of $O{=}Fe^{IV}$TpivPP. This was a typical electrocatalytic process,[50] in which Fe^{III}TpivPP was first oxidized to the iron(IV) species and then back to the initial state by a chemical reaction according to the oxygen-atom-transfer mechanism of a high-valent porphyrin [Eq. (2)].[48]

$$2\,O{=}Fe^{IV}TpivPP + SO_3^{2-} + H_2O \rightarrow 2\,HO{-}Fe^{III}TpivPP + SO_4^{2-} \quad (2)$$

The oxidation potential of the sulfite ions was much more negative than for GCEs modified with diazo resins/anionic iron(III) tetrakis(*p*-sulfonatophenyl)porphyrin (pH 8.74, +0.82 V),[51] and GCEs modified with iron(III) tetra(4-aminophenyl)porphyrin (pH 9.55, +0.83 V).[49] Thus, the as-prepared nanocomposite showed increased electrocatalytic ability for the oxidation of sulfite ions. The low overpotential was beneficial in excluding the interference of other reductive species that coexisted in the samples.

Although the proton did not participate in the oxidation of sulfite ions by iron(IV) species, the catalytic peak potential for the oxidation of sulfite ions shifted on increasing from pH 5 to 9 to more a negative value with a slope of −56.9 mV pH^{-1} (Figure 7A), which is consistent with the generation of iron(IV) species. This result further indicated a one-proton and one-electron redox process for the generation of iron(IV) species, which led to the dependence of the peak current of the oxidation of sulfite ions on pH value (Figure 7B).

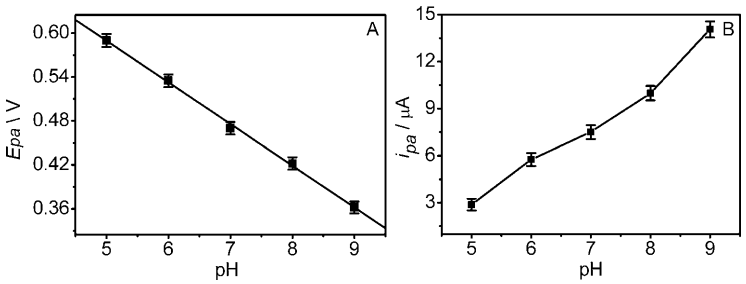

Figure 7. Effects of pH value on A) oxidation peak potential and B) current of sulfite ions (500 μmol L^{-1}) in 0.1 M PBS. Scan rate: 100 mV s^{-1}.

Amperometric biosensing of sulfite ions: The current/time curve of the CN_x MWNT/FeTpivPP-modified GCE upon successive addition of sulfite ions at an applied potential of +0.47 V clearly illustrated that the modified GCE could respond very rapidly to the change in the sulfite concentration (Figure 8). The response reached a steady signal within only 3 seconds and displayed a linear increase with the increasing concentration from 8.0×10^{-7} to 4.9×10^{-3} mol L^{-1}, with a detection limit of 3.5×10^{-7} mol L^{-1} at a signal-to-noise ratio of 3:1. The linear response range was wider than 6×10^{-6}–1×10^{-3} mol L^{-1} at the carbon ionic liquid electrode[52] and 4×10^{-6} –6.9×10^{-5} mol L^{-1} at the electrode modified with nanostructured copper–salen polymer film.[53] Also, the detection limit was lower than 4×10^{-6} and 1.2×10^{-6} mol L^{-1}[52,53] at the above respective modified electrodes. Thus, the biosensor showed a good performance for the determination of sulfite ions due to the highly efficient catalysis of the CN_x MWNT/FeTpivPP nanocomposite.

The sulfite biosensor showed good fabrication reproducibility with a relative standard deviation of 4.3% estimated from the slopes of the calibration plots at five freshly prepared CN_x MWNT/FeTpivPP-modified GCEs. At the concentrations of 8 and 800 μmol L^{-1} for the sulfite ions, the

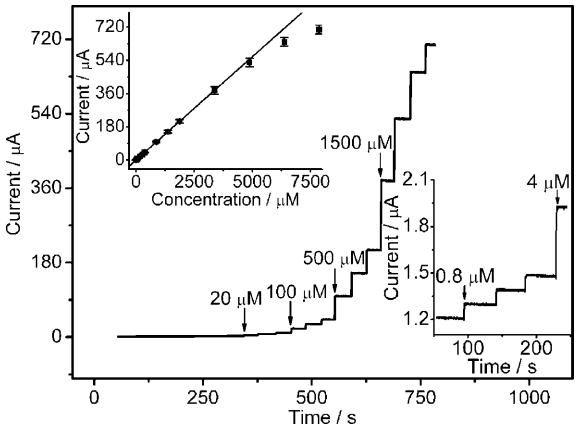

Figure 8. Successive amperometric response of the CN_x MWNT/FeTpivPP-modified GCE to sulfite ions in PBS (0.1 M, pH 7.0) at an applied potential of +0.47 V. Upper inset: linear calibration curve; lower inset: amplified response.

biosensor showed good repeatability with relative standard deviations of 4.7 and 4.0% examined over five determinations, respectively. At the sulfite concentration of 500 μmol L^{-1}, the cyclic voltammogram of the biosensor for consecutive fifty scans between −0.6 and 0.9 V showed acceptable stability. The response of the sulfite ions at the fiftieth scan remained 98.2% of its initial response. When the biosensor was not in use, it was stored in the shade at room temperature and measured every few days. No obvious decrease in the amperometric response to sulfite ions was observed after one week of storage. The biosensor could keep 95.3% of its initial amperometric response after four weeks. This result implied that the structure of the CN_x MWNT/FeTpivPP film was very efficient for retaining the activity of FeTpivPP and preventing it from leaking out of the biosensor.

Interference study and detection of sulfite ions in real samples: The effects of common interfering species on the biosensor response were examined. The detection potential of +0.47 V, a more negative value than applied at other amperometric biosensors for sulfite ions, avoided the interference of electrochemically reductive compounds. For example, anions (F^-, Br^-, Cl^-, NO_2^-, NO_3^-, CO_3^{2-}, HCO_3^-, PO_3^{3-}, HPO_3^{2-}, $H_2PO_3^-$), organic acids (lactic acid, tartaric acid, citric acid, oxalic acid), and saccharides (sucrose, glucose, fructose) at 1000-fold concentrations of the sulfite ions did not interfere with the amperometric response of the sulfite ions. Ascorbic acid was tolerated at less than a threefold concentration of sulfite ions. Sulfide ions at the same concentration as the sulfite ions interfered with the amperomet-

ric response of the sulfite ions; however, this response did not occur with sulfite ions in food and beverage samples. Thus, the present biosensor could be applied successfully to the determination of sulfite ions without any sample pretreatment. The amperometric biosensor had excellent specificity for the highly sensitive detection of sulfite ions in food and beverage samples.

The concentration of sulfite ions in grape juice was detected with the proposed biosensor to be $5.3 \pm 0.2\ \mu mol\,L^{-1}$ (five measurements) without any need for sample pretreatment. This value was close to $5.0\ \mu mol\,L^{-1}$ as measured by the standard iodimetric method. Recovery testing was further carried out to demonstrate the validity of the proposed method. After sulfite ions (8 and $800\ \mu mol\,L^{-1}$) were added to this sample, the obtained recoveries of sulfite ions were 105.2 ± 2.8 and $97.1 \pm 2.5\,\%$, respectively.

Conclusions

A water-insoluble picket-fence porphyrin was first assembled on nitrogen-doped multiwalled carbon nanotubes (CN_x MWNTs) through Fe–N coordination for the preparation of highly efficient catalysts. Direct electrochemistry that corresponds to the redox couple of Fe^{III}/Fe^{II} was realized. The oxidation of the assembled porphyrin at low potential formed a high-valent iron(IV)–porphyrin. The CN_x MWNT/FeTpivPP-modified electrode showed excellent catalytic activity toward the electrooxidation of sulfite ions mediated by iron(IV) species with low overpotential, thus leading to good analytical performance in the detection of sulfite ions, such as a rapid response, wide linear range, low detection limit, good fabrication reproducibility, and acceptable accuracy. The direct noncovalent assembly of porphyrins on nitrogen-doped carbon nanotubes provides a facile way to design novel biofunctional materials for biosensing and photovoltaic devices.

Experimental Section

Materials and reagents: Nitrogen-doped multiwalled carbon nanotubes (CN_x MWNTs) with a nitrogen content of 4.6 % were synthesized according to previous reports[19,54] and were further heated to reflux in NaOH ($6\ mol\,L^{-1}$) at 110 °C for 4 h to remove the Al_2O_3 support, followed by heating to reflux in H_2SO_4 ($1\ mol\,L^{-1}$) for 8 h to remove the residual Fe catalysts. The purified CN_x MWNTs were thoroughly washed with double-distilled water until the filtrate reached pH 7 and were dried at 70 °C overnight.

Bromo[iron(III) 5,10,15,20-tetrakis(α,α,α,α-2-pivalamidopheny)porphyrin] (FeTpivPP) and the corresponding free-base porphyrin were prepared according to procedures in previous reports.[44] Multiwalled carbon nanotubes (MWNTs) (>95 %; diameter: 20–40 nm) were purchased from Shenzhen Nanotech Port Ltd. Co. (China), anhydrous sodium sulfite (>97.0 %) was purchased from Nanjing Chemical Reagent Co. Ltd. (China), and all the other chemicals were of analytical grade. Aqueous solutions were prepared with double-distilled water. Phosphate buffered saline (PBS) ($0.1\ mol\,L^{-1}$) was always employed as the supporting electrolyte, which was deaerated with high purity nitrogen for 20 min. The pH value of PBS was pH 7.0, except in those cases indicated.

Apparatus: Scanning electron micrographs were obtained by using a Hitachi S-4800 scanning electron microscope (Hitachi, Japan). Resonance Raman spectra were recorded on a Renishaw-inVia Raman microscope (Renishaw, UK). X-ray photoelectron spectroscopic measurements were performed with an ESCALAB 250 spectrometer (Thermo-VG Scientific, USA) with ultrahigh vacuum generator. UV/Vis absorption spectra were recorded with a Lambda 35 UV/VIS spectrometer (Perkin–Elmer, USA). Electrochemical impedance spectroscopic measurements were carried out on a PGSTAT30/FRA2 system (Autolab, the Netherlands) in KCl solution ($0.1\ mol\,L^{-1}$) containing $K_3[Fe(CN)_6]$ ($5\ mmol\,L^{-1}$)/$K_4[Fe(CN)_6]$ ($5\ mmol\,L^{-1}$). The impedance spectra were recorded at 10^{-2}–10^5 Hz. The amplitude of the applied sine wave potential in each case was 5 mV. Cyclic voltammetry and amperometric experiments were preformed on a CHI 812B electrochemical workstation (CH Instruments Inc., USA). All the experiments were carried out at room temperature with a conventional three-electrode system with a modified glassy carbon electrode, a platinum wire, and a saturated calomel electrode as the working, auxiliary, and reference electrodes, respectively.

Preparation of CN_x MWNTs/FeTpivPP-modified GCE: CN_x MWNTs (15 mg) in THF (5 mL) were successively added to FeTpivPP in THF (1.5 mL, $1\ mg\,mL^{-1}$). The resulting suspension was ultrasonically dispersed for 1 h and centrifuged at 10000 rpm for 15 min to remove free FeTpivPP. After washing with THF (5×), the sediment was dried at 70 °C to obtain the CN_x MWNTs/FeTpivPP nanocomposite. The as-prepared nanocomposite was ultrasonically dispersed to obtain a suspension of CN_x MWNTs/FeTpivPP in THF ($0.5\ mg\,mL^{-1}$).

The GCEs (diameter: 3 mm) were polished to a mirror finish with an alumina slurry (1.0 and 0.05 μm) on chamois leather, ultrasonically washed in absolute ethanol and double-distilled water for 2 min, respectively, and dried at room temperature. A suspension of CN_x MWNTs/FeTpivPP in THF (5 μL, $0.5\ mg\,mL^{-1}$) was applied to the GCE and dried at room temperature to obtain the CN_x MWNTs/FeTpivPP-modified electrode. Similarly, a CN_x MWNT-modified GCE was prepared.

Acknowledgements

This study was supported by the National Basic Research Program of China (2010CB732400), the Funds for Creative Research Groups (20821063), Major Research Plan (90713015), Key (20535010, 20835006) and General (20875044, 20745003, 20705012) Programs from the NSFC, PhD Fund for Young Teachers (20070284052), and Science Foundation of Jiangsu (BK2007570, BK2008014).

[1] V. Sgobba, D. M. Guldi, *Chem. Soc. Rev.* **2009**, *38*, 165.
[2] D. Baskaran, J. W. Mays, X. P. Zhang, M. S. Bratcher, *J. Am. Chem. Soc.* **2005**, *127*, 6916.
[3] Z. B. Liu, J. G. Tian, Z. Guo, D. M. Ren, F. Du, J. Y. Zheng, Y. S. Chen, *Adv. Mater.* **2008**, *20*, 511.
[4] G. M. A. Rahman, A. Troeger, V. Sgobba, D. M. Guldi, N. Jux, D. Balbino, M. N. Tchoul, W. T. Ford, A. Mateo-Alonso, M. Prato, *Chem. Eur. J.* **2008**, *14*, 8837.
[5] D. M. Guldi, G. M. A. Rahman, M. Prato, N. Jux, S. H. Qin, W. Ford, *Angew. Chem.* **2005**, *117*, 2051; *Angew. Chem. Int. Ed.* **2005**, *44*, 2015.
[6] D. M. Guldi, G. M. A. Rahman, F. Zerbetto, M. Prato, *Acc. Chem. Res.* **2005**, *38*, 871.
[7] D. S. Hecht, R. J. A. Ramirez, M. Briman, E. Artukovic, K. S. Chichak, J. F. Stoddart, G. Grüner, *Nano Lett.* **2006**, *6*, 2031.
[8] T. Hasobe, S. Fukuzumi, P. V. Kamat, *J. Am. Chem. Soc.* **2005**, *127*, 11884.
[9] M. Alvaro, P. Atienzar, P. D. L. Cruz, J. L. Delgado, V. Troiani, H. Garcia, F. Langa, A. Palkar, L. Echegoyen, *J. Am. Chem. Soc.* **2006**, *128*, 6626.
[10] J. X. Yu, S. Mathew, B. S. Flavel, M. R. Johnston, J. G. Shapter, *J. Am. Chem. Soc.* **2008**, *130*, 8788.

[11] R. Chitta, A. S. D. Sandanayaka, A. L. Schumacher, L. D′Souza, Y. Araki, O. Ito, F. D′Souza, *J. Phys. Chem. C* **2007**, *111*, 6947.
[12] K. P. Gong, F. Du, Z. H. Xia, M. Durstock, L. M. Dai, *Science* **2009**, *323*, 760.
[13] R. Czerw, M. Terrones, J. C. Charlier, X. Blase, B. Foley, R. Kamalakaran, N. Grobert, H. Terrones, D. Tekleab, P. M. Ajayan, W. Blau, M. Rühle, D. L. Carroll, *Nano Lett.* **2001**, *1*, 457.
[14] J. C. Carrero-Sánchez, A. L. Elías, R. Mancilla, G. Arrellín, H. Terrones, J. P. Laclette, M. Terrones, *Nano Lett.* **2006**, *6*, 1609.
[15] A. L. Elías, J. C. Carrero-Sánchez, H. Terrones, M. Endo, J. P. Laclette, M. Terrones, *Small* **2007**, *3*, 1723.
[16] X. Lepró, Y. Vega-Cantú, F. J. Rodríguez-Macías, *Nano Lett.* **2007**, *7*, 2220.
[17] Q. H. Yang, P. X. Hou, M. Unno, S. Yamauchi, R. Saito, T. Kyotani, *Nano Lett.* **2005**, *5*, 2465.
[18] M. Dehonor, K. Masenelli-Varlot, A. González-Montiel, C. Gauthier, J. Y. Cavaillé, H. Terronesa, M. Terrones, *Chem. Commun.* **2005**, 5349.
[19] B. Yue, Y. W. Ma, H. S. Tao, L. S. Yu, G. Q. Jian, X. Z. Wang, X. S. Wang, Y. N. Lu, Z. Hu, *J. Mater. Chem.* **2008**, *18*, 1747.
[20] J. P. Collman, R. Boulatov, C. J. Sunderland, L. Fu, *Chem. Rev.* **2004**, *104*, 561.
[21] T. S. Balaban, M. Linke-Schaetzel, A. D. Bhise, N. Vanthuyne, R. Christian, C. E. Anson, G. Buth, A. Eichhöfer, K. Foster, G. Garab, H. Gliemann, R. Goddard, T. Javorfi, A. K. Powell, H. Rösner, T. Schimmel, *Chem. Eur. J.* **2005**, *11*, 2267.
[22] I. M. Wasser, H. W. Huang, P. Moënne-Loccoz, K. D. Karlin, *J. Am. Chem. Soc.* **2005**, *127*, 3310.
[23] G. M. A. Rahman, A. Troeger, V. Sgobba, D. M. Guldi, N. Jux, D. Balbino, M. N. Tchoul, W. T. Ford, A. Mateo-Alonso, M. Prato, *Chem. Eur. J.* **2008**, *14*, 8837.
[24] W. W. Tu, J. P. Lei, L. Ding, H. X. Ju, *Chem. Commun.* **2009**, 4227.
[25] W. W. Tu, J. P. Lei, H. X. Ju, *Chem. Eur. J.* **2009**, *15*, 779.
[26] B. Steiger, F. C. Anson, *Inorg. Chem.* **2000**, *39*, 4579.
[27] J. P. Collman, R. Boultaov, C. J. Sunderland, I. M. Shiryaeva, K. E. Berg, *J. Am. Chem. Soc.* **2002**, *124*, 10670.
[28] J. P. Lei, H. X. Ju, O. Ikeda, *J. Electroanal. Chem.* **2004**, *567*, 331.
[29] A. Takahashi, T. Kurahashi, H. Fujii, *Inorg. Chem.* **2009**, *48*, 2614.
[30] J. P. Collman, Y. L. Yan, J. P. Lei, P. H. Dinolfo, *Inorg. Chem.* **2006**, *45*, 7581.
[31] J. P. Collman, N. K. Devaraj, R. A. Decréau, Y. Yang, Y. L. Yan, W. Ebina, T. A. Eberspacher, C. E. D. Chidsey, *Science* **2007**, *315*, 1565.
[32] S. Yoshimoto, K. Sato, S. Sugawara, Y. Chen, O. Ito, T. Sawaguchi, O. Niwa, K. Itaya, *Langmuir* **2007**, *23*, 809.
[33] R. Walker, *Food Addit. Contam.* **1985**, *2*, 5.
[34] M. Situmorang, D. B. Hibbert, J. J. Gooding, D. Barnett, *Analyst* **1999**, *124*, 1775.
[35] H. Vally, A. Carr, J. El-Saleh, P. Thompson, *J. Allergy Clin. Immunol.* **1999**, *103*, 41.
[36] H. Vally, P. Thompson, *Thorax* **2001**, *56*, 763.
[37] Federal Register, *Food Labeling: Declaration of Sulfiting Agents*, **1986**, *51*, 25012.
[38] Federal Register, *Sulfiting Agents: Revocation of GRAS Status for Use on Fruits and Vegetables Intended To Be Sold Raw to Consumers*, **1986**, *51*, 25021.
[39] X. B. Yan, B. K. Tay, Y. Yang, *J. Phys. Chem. B* **2006**, *110*, 25844.
[40] Q. Yang, L. Shuai, J. J. Zhou, F. C. Lu, X. J. Pan, *J. Phys. Chem. B* **2008**, *112*, 12934.
[41] P. Ghosh, M. Zamri, M. Subramanian, T. Soga, T. Jimbo, R. Katoh, M. Tanemura, *J. Phys. D* **2008**, *41*, 155405.
[42] P. Ayala, A. Grüneis, T. Gemming, B. Büchner, M. H. Rümmeli, D. Grimm, J. Schumann, R. Kaltofen, F. L. F. Jr, H. D. F. Filho, T. Pichler, *Chem. Mater.* **2007**, *19*, 6131.
[43] S. Maldonado, S. Morin, K. J. Stevenson, *Carbon* **2006**, *44*, 1429.
[44] J. P. Collman, R. R. Gagne, C. A. Reed, T. R. Halbert, G. Lang, W. T. Robinson, *J. Am. Chem. Soc.* **1975**, *97*, 1427.
[45] J. Y. Chen, C. P. Collier, *J. Phys. Chem. B* **2005**, *109*, 7605.
[46] M. Lefèvre, J. P. Dodelet, P. Bertrand, *J. Phys. Chem. B* **2002**, *106*, 8705.
[47] Y. Liu, Y. L. Yan, J. P. Lei, F. Wu, H. X. Ju, *Electrochem. Commun.* **2007**, *9*, 2564.
[48] H. Fujii, *Coord. Chem. Rev.* **2002**, *226*, 51.
[49] M. Luceroa, G. Ramíreza, A. Riquelmea, I. Azocara, M. Isaacsa, F. Armijoa, J. E. Förstera, E. Trollunda, M. J. Aguirrea, D. Lexab, *J. Mol. Catal. B J. Mol. Catal. A J. Mol. Catal. A - Chem.* **2004**, *221*, 71.
[50] A. J. Bard, L. R. Faulkner, *Electrochemical Methods*, John Wiley & Sons, Inc., New York, **2001**, pp. 473–475.
[51] X. F. Li, Y. Q. Fu, C. Q. Sun, *Electroanalysis* **2003**, *15*, 1707.
[52] A. Safavi, N. Maleki, S. Momeni, F. Tajabadi, *Anal. Chim. Acta* **2008**, *625*, 8.
[53] T. R. L. Dadamos, M. F. S. Teixeira, *Electrochim. Acta* **2009**, *54*, 4552.
[54] H. Chen, Y. Yang, Z. Hu, K. F. Huo, Y. W. Ma, Y. Chen, *J. Phys. Chem. B* **2006**, *110*, 16422.

Received: October 18, 2009
Published online: February 16, 2010

